Multichord optical interferometry of FRX-L's field reversed configuration

E. L. Ruden[a)]
Air Force Research Laboratory, Directed Energy Directorate, Kirtland AFB, New Mexico 87117

Shouyin Zhang, G. A. Wurden, T. P. Intrator, R. Renneke, and W. J. Waganaar
Los Alamos National Laboratory, Los Alamos, New Mexico 87545

F. T. Analla and T. C. Grabowski
Science Applications International Corporation, Albuquerque, New Mexico 87106

A 0.633 μm laser interferometer provides detailed time resolved information about the spatial distribution of the plasma density of field reversed configurations (FRC's) produced by the FRX-L experiment at Los Alamos National Laboratory. This experiment is an effort to produce a magnetized plasma with closed field lines suitable for compression by a solid metal liner imploded by the Shiva Star capacitor bank at the Air Force Research Laboratory. The interferometer probes a fanned array of eight chords through the FRC midplane, measuring the line integrated free electron density via its effect on optical phase shift relative to eight reference beams as a function of time. The reference beams are given nominally identical optical paths, except that they are folded for compactness and given an 80 MHz higher optical frequency by use of a Bragg cell beam splitter. After the beams are recombined, interference results in 80 MHz electromagnetic beat waves with dynamic phase shifts equal to those of the corresponding optical probes. Quadrature mixing of the electronically monitored light is then performed with rf components. Noteworthy features of the interferometer's design are the unique compact folding scheme of the reference paths, inclusion of a fused quartz tube in the reference path similar to that of the FRC's vacuum vessel to compensate for cylindrical lensing, and transmission of the interfering light via optical fibers to a rf shielded room for processing. Extraneous contributions to the phase shift due to vibration resulting from the system's pulsed magnetic field, and dynamic refractive changes in or near the fused quartz tube wall (possibly due to radiation heating) are corrected for. © *2006 American Institute of Physics.*
[DOI: 10.1063/1.2354568]

I. INTRODUCTION

The field reversed configuration (FRC) experiment with a liner (FRX-L) interferometer measures the line integral of plasma density along eight probe beams transmitted through the plasma chamber as a function of time. It is a reliable and useful instrument with a unique design and versatile layout that may be useful for other applications. Density profiles during the azimuthally symmetric phase have been inferred by Abel inversion,[1] and, correlated with other diagnostics, critical confinement information has been inferred.[2] As with most FRC experiments,[3] an instability with azimuthal mode number $n=2$ develops after formation, terminating the symmetric phase. The instability is observed to grow rapidly into a saturated state that appears to rotate approximately as a rigid rotor, except for a gradual, roughly linear, loss in overall density. After decay correction, a sufficient data set has been obtained for a full two-dimensional tomographic inversion of the midplane density profile by interpreting phase shift measurements from the eight channels at different times as line integrated measurements of a fixed density profile rotated at different angles. Understanding and controlling this instability is of critical importance to the magnetized

target fusion application of FRX-L, but this article will focus on the instrument itself and on data analysis to the point of inferring the contribution of phase shift due to plasma dispersion. Abel and tomographic inversion procedures and results, in addition to FRC properties that may thereby be inferred, are presented in detail in a complementary paper simultaneously submitted to Physics of Plasmas.

The FRC is formed within a fused quartz tube initially filled with D_2 gas by four coordinated circuits which impose various magnetic field components to form and subsequently confine the FRC. A detailed description of the FRX-L FRC formation hardware and pulsed power circuit is available elsewhere.[4] All results presented here are for a single representative shot (No. 3213) and its corresponding vacuum reference shot (No. 3205, without prefill) needed to measure the interferometer's acoustic response to the machine's firing. For comparison with other published results, the "main" magnetic reversal, preionization, bias, and cusp/mirror magnetic field circuit capacitor charge voltages for this shot are 70, 30, 8.7, and 8.5 kV, respectively. The main bank trigger delay relative to application of the bias current and the delay between the main bank discharge and its associated crowbar switch trigger are 137.8 and 2.7 μs, corresponding to the quarter-cycle rise times of the bias and main magnetic fields,

---
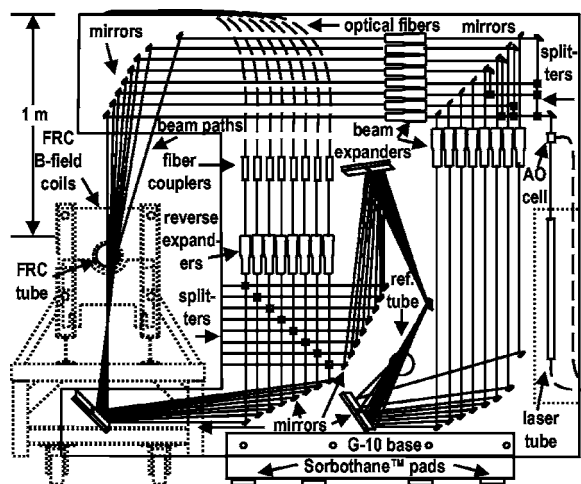
a)Electronic mail: edward.ruden@kirtland.af.mil

FIG. 1. Scale drawing of multichord interferometer and its optical beam path as fielded on the FRX-L (shown end-on in dotted outline) FRC midplane.

respectively. The high frequency (250 kHz) preionization circuit is triggered 23 μs before the main bank. The D_2 prefill pressure is 50.4 mtorr.

II. HARDWARE

The interferometer elements, schematically illustrated in Fig. 1, are mounted on a 10 cm thick honeycomb-reinforced SS304 stainless steel rectangular breadboard with a rectangular cutout to accommodate the FRC formation chamber. The breadboard is supported vertically by a base constructed from 10 cm thick G-10 fiber glass plates resting on 2.5 cm thick Sorbothane™ (low elastic modulus polyurethane) pads on a concrete first floor foundation. The optical components are enclosed by a Lexan™ dust cover purged by filtered air impelled by a squirrel cage blower with an external motor isolated from the air stream (to minimize air heating). Air flowing over copper foil heat exchangers attached to the laser tube (mounted on the breadboard) is contained within a small partitioned volume enclosing the tube to isolate it from the rest of the breadboard. It was found that heat from either a rotary fan motor or the laser tube, if not managed in this way, will deform the breadboard sufficiently to disturb alignment. To avoid the effects of radio frequency (rf) noise produced by the machine, the laser tube and its high voltage cable are enclosed in a copper braided tube clamped to a solid copper feedthrough tube entering a power-filtered rf-tight enclosure containing the laser power supply. The enclosure is powered externally by a battery powered uninterruptable power supply, which is unplugged from the wall during the shot. Nonconducting or, where not possible, nonmagnetic materials are used to minimize the Lorentz force interaction with the pulsed magnetic field produced by the experiment. Acrylic was used for the breadboard initially for this reason, but proved too dimensionally unstable for alignment to be preserved for more than a few hours.

The interferometer probes eight chords through the FRC midplane, as illustrated in Fig. 1. It uses a single 23 mW 0.633 μm linearly polarized He–Ne laser as the source for all probe and reference beams. The geometry is essentially

Mach-Zehnder, except that it has multiple paths folded for compactness and, rather than using a traditional beam splitter to separate the initial beam into probe and reference branches, a flint glass acousto-optic Bragg cell driven by an 80 MHz piezoelectric splits off half the initial beam power by diffraction to supply the reference beams. The reference beams' optical frequency is thereby Doppler shifted by 80 MHz, allowing quadrature mixing (needed to determine phase shift unambiguously) to be performed with rf components. To create eight probe and matching reference beams, an array of cubic beam splitters is used to split both probe and reference beams into halves, then quarters, and then eighths. The angle of separation of the original probe and reference beams is sufficiently small (14.4 mrad) that this subsequent splitting is performed for both by the same cubic splitters. Thereafter, the reference beams are individually picked off by mirrors and sent to matched reference paths.

Beam expanders are used to expand the individual channel probe and reference beams by a factor of 6 to about 1 cm diameter and focus them to a diffraction limited waist within the fused quartz FRC formation tube at an optical distance of about 2 m. Such focusing mitigates refractive distortion due to substantial azimuthal ripples in the fused quartz tube wall. The laser plane of polarization is chosen to be normal to the tube's z axis to maximize the transmission coefficient of beams probing chords of high impact parameter (minimum distance to z axis). A similar, but truncated, fused quartz tube placed in the reference beams' paths matches the cylindrical lensing and slight refractive deflection of the beams due to passage through the tube wall. Chordal impact parameters up to 95% of the tube's inner radius may thereby be successfully probed, based on bench tests. The tube's inner and outer radii are 5.25 and 5.47 cm, respectively.

The probe beams pass through laser line filters after traversing the FRC chamber to minimize plasma light transmission. They are then recombined with their respective reference beams by cubic beam splitters and fed into multimode optical fibers via reversed $6\times$ beam expanders followed (after a distance) by converging lenses on the fiber mounts. The reference beams are provided a nominally identical optical path, except, of course, for the absence of plasma, although they are folded up to save space. Intensity modulated light with a base line frequency of 8 MHz results when each probe and reference beam interferes due to the electromagnetic beat wave that results from the higher optical frequency of the latter. The time dependent electromagnetic phase shift of each probe beam relative to its reference beam equals the phase shift of this beat wave from its 80 MHz base line.

The optical fibers transport the interfering light to a remote rf shielded room where the intensity modulated light is converted to phase modulated 80 MHz rf signals by optical receivers. The rf signals are mixed by in-phase quadrature (IQ) demodulators with 80 MHz local oscillator (LO) signals split off from the Bragg cell driver. An IQ demodulator has two outputs proportional to the sine and cosine of the phase shift between the rf and LO inputs. This phase shift is, in our geometry, equal to that of the corresponding probe beam relative to its reference beam. Subsequent 60 MHz low-pass filters remove high frequency leakage and upper band inter-
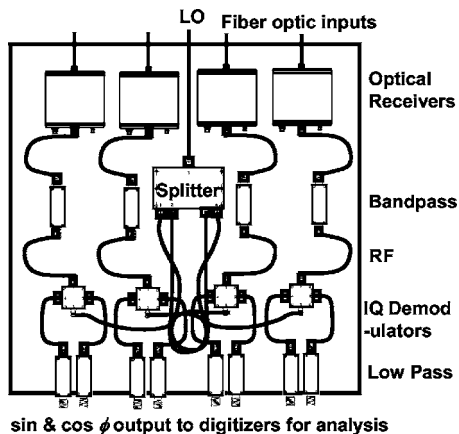
FIG. 2. Layout for one of two four-channel demodulator circuit panels that receive the fiber optic outputs from the interferometer (Fig. 1). Components are mounted on an 18 in. wide relay rack pull-out shelf.
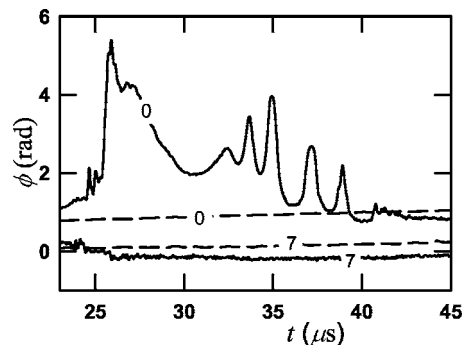

FIG. 3. Uncorrected phase shift vs time for channels 0 and 7 (solid lines) of a representative shot, with corresponding vacuum reference shot signals overlaid (dashed lines). Note that channel 7's trace, whose chord does not intercept the FRC plasma, is well below its vacuum reference, indicating that it is responding to an index change opposite to that of plasma from a source outside the FRC. It is presumed to be localized in the vicinity of the fused quartz FRC tube wall.

ference from the demodulator outputs and define the instrument's diagnostic bandwidth. The component layout for one of two four-channel circuit panels that perform the above is illustrated in Fig. 2.

The reversed beam expanders described above are used to focus the interfering probe and reference light into narrow (~3 mm) collimated beams which traverse sufficient distance (~30 cm) to allow the beams to be overlapped by eye accurately enough to produce initial interference signals. Each channel's optical receiver output is then optimized by iterative adjustments of the recombining beam splitter and final probe steering mirror mounts while observing its amplitude on an oscilloscope.

III. PHASE SHIFT MEASUREMENT AND CORRECTIONS

The two IQ demodulator output signals for each channel probe are recorded by transient digitizers and numerically converted to phase shift ϕ versus time t from the (multivalued) arctangent of the ratio. The phase shift quadrant is determined by using a two argument arctangent function that considers the signs of these two arguments (numerator and denominator) separately to give a result between $-\pi$ and π. The order of shift (the multiple of 2π that must be added to ϕ) is tracked by cumulatively adding or subtracting 2π to ϕ whenever the two argument arctangent changes by more than $-\pi$ or π, respectively, between time samples. Boxcar smoothing is generally used beforehand, though, to avoid false triggering of the order change. After $\phi(t)$ is determined in this way, its initial recorded value is subtracted so that ϕ is defined to start at zero. Results for two channels of the representative FRC formation shot are plotted in Fig. 3. All probe beams cross below the quartz tube at a distance $c_k = 30.6$ cm from the z axis. Impact parameters are, for probes $\{k\}$,

$$\{r_k, k = 0, 1, \ldots, 7\}$$

$$= \{0.0, 0.7, 1.8, 2.4, 2.9, 3.5, 3.7, 4.1\} \text{ cm.} \quad (1)$$

Operationally, $\{c_k\}$ values are set and measured directly for both reference and probe paths. $\{r_k\}$ values, however, are set

and measured directly only for the reference paths due to access limitations within the FRC tube. Matching $\{r_k\}$ values for the probe paths are assured by carefully matching the positions of laser transmission and reflection spots on the various lenses and mirrors, respectively, mounted to the optical table.

Two significant time dependent contributions to ϕ are observed in addition to refraction from the FRC plasma which must be subtracted to obtain the latter. The first results from geometrical beam path length changes due to acoustic vibrations of the (conducting) 304 stainless steel breadboard imparted by interaction with the (slow) pulsed magnetic bias field. This contribution is measured by periodically firing the bias field under similar experimental conditions, but without a gas prefill (vacuum only). Figure 3 overlays the vacuum shot traces used to correct the representative shot for channels 0 and 7 only (to avoid congestion) to illustrate the magnitude and low frequency nature of this effect.

The second non-FRC plasma ϕ contribution occurs only when the FRC is formed, but results from a source well outside the FRC separatrix, based on the outermost (exterior) chord, 7 (which is well outside the separatrix after the initial stages of FRC formation). This contribution is of opposite sign to the plasma induced phase shift, builds up slowly during the plasma discharge, and plateaus to a constant value as the plasma decays. This gradual cumulative behavior and the observed chordal dependence are consistent with a slight bulk heating of the fused quartz by direct radiation absorption within the spectral range of 0.2–0.3 μm where the fused quartz is neither strongly transmitting nor absorbing (the latter of which would only result in heating and/or ablating the inner surface). Neglecting thermal expansion

$$\lambda_0 \phi_{i,w} = -2\pi \eta_1 L_i \Delta T \quad (2)$$

in the thin shell limit, where $\lambda_0 = 0.633$ μm is the laser wavelength, $\phi_{i,w}$ is the phase shift due to wall heating for probe i, $\eta_1 = 1.01 \times 10^{-5}$ K^{-1} is the first derivative of the fused quartz's index of refraction at room temperature[5] versus temperature, L_i is the distance the beam probing chord i travels through fused quartz ($L_7 = 4.5$ mm, for example), and ΔT is the tube's thickness-averaged temperature change. From this,
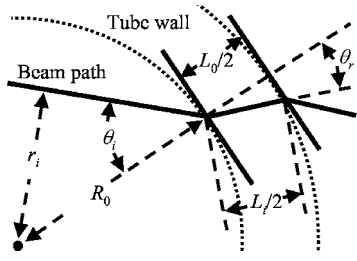
FIG. 4. Model geometry (not to scale) used to estimate the path length of the laser beam through the fused quartz tube wall L_i for the purposes of correcting for refractive index changes therein. The tube wall is locally approximated as a flat plate of thickness L_0, as drawn.
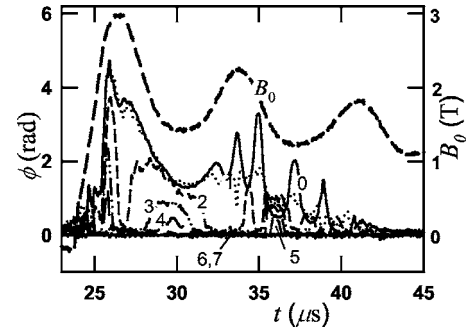

FIG. 5. The representative shot's phase shift history for channels 0–7 (as labeled), with each channel's corresponding vacuum reference signal and wall phase shift perturbation (based on channel 7) subtracted. B_0, the vacuum external B_z near the FRC midplane, is overlaid for reference. Channels 6 and 7 traces are very small and difficult to distinguish. Time $t=0$ (off scale) corresponds to the triggering of the 250 kHz preionization circuit.

the value $\phi_{7,w} = -0.3$ rad observed at the end of the trace in Fig. 3 would result from $\Delta T = 0.7$ K. By convention, we *define* the phase shift due to plasma as being positive. Since the index of refraction of the plasma is *less than* 1 (Ref. 6) in our regime (above the plasma frequency, where polarization opposes the electric field), a positive index change results in a negative phase shift in Eq. (2). The effect of the thermal expansion coefficient on L_i has been neglected here since this coefficient is 20 times smaller than η_1 for fused quartz. For many glasses, though, it may be significant.

Assuming azimuthal symmetry in ΔT, Eq. (2) implies $\phi_{i,w} = \phi_{7,w} L_i / L_7$. Ignoring tube wall curvature effects, L_i may be estimated by approximating the tube wall in the vicinity of either of the beam's two traverses into or out of the tube interior as a flat plate of thickness $L_0/2$, as illustrated in Fig. 4. This model plate is presumed to have a point of minimum distance R_0 from the tube axis coinciding with the point where chord i intersects the interior plate surface. $R_0 = 5.25$ cm is the tube's inner radius. If we further assume that chord 7 lies outside the FRC plasma so that, after vacuum signal subtraction, $\phi_7 = \phi_{7,w}$, one finds the following from Snell's law:

$$\phi_{i,w} = \phi_7 \sqrt{\frac{(\eta_0 R_0)^2 - r_7^2}{(\eta_0 R_0)^2 - r_i^2}}, \tag{3}$$

where $\eta_0 = 1.46$ is the nominal index of refraction of fused quartz.

In practice, vacuum and wall contributions, being relatively low in frequency, are smoothed significantly to minimize noise. Once subtracted, the remaining phase shift ϕ contribution from the FRC plasma proper is best approximated by[7]

$$A\phi = \int_{\substack{\text{beam} \\ \text{path}}} n_e dl, \tag{4}$$

where n_e is plasma free electron density *interior to the FRC and after formation*, dl is the increment of path length of the laser beam, and, for $\lambda_0 = 0.633 \ \mu$m, $A = 5.61 \times 10^{16}$ cm²/rad. Figure 5 plots the results. B_0, B_z as recorded by a B-dot probe just external to the fused quartz tube and near the FRC midplane, is overlaid for reference.

IV. DISCUSSION

Equation (3) is not applicable during the preionization phase since plasma is distributed beyond chord 7 then. Even

beyond this phase, there may be an additional contribution to ϕ_7 from initially adsorbed gas and/or quartz constituents (ionized or otherwise) ablated from the tube's inner surface. Such material is seen in end-on visible light imaging and appears concentrated near the wall.[8] Being localized there, its chordal dependence would be similar to Eq. (3), but with (base line index) $\eta_0 = 1$. Fortunately, the dependence on η_0 is not very strong, so Eq. (3) automatically accounts for this contribution too, for the most part. The difference in $\phi_{i,w}$ between $\eta_0 = 1.46$ and $\eta_0 = 1$ is less than 0.07 rad for ϕ_7 of the presented data, for example. The wall effect is more pronounced for more recent results (not reported here), and subtracting Eq. (3) with $\eta_0 = 1.46$ from (vacuum signal corrected) ϕ_i results in it returning to zero at a later time more accurately than with $\eta_0 = 1$, at least averaged over several shots and/or channels. For any particular channel of any particular shot, the difference is inconclusive due to shot-to-shot variation in the vacuum reference signal (which must be subtracted first) of roughly 0.1 rad, which limits the degree to which the corrected phase shifts return to zero after FRC decay. A definitive confirmation of the bulk heating of the wall material by plasma radiation from the FRC and wall ablated plasma in the near UV band where fused quartz neither absorbs nor transmits strongly would require a measurement of the near UV power spectrum of light shining through the fused quartz tube in the region of its UV cutoff. One may then retrodict the wall effect measurement from this and fused quartz's known wavelength dependent absorption coefficient. Short of this, the wall heating basis of Eq. (3) has nonetheless been proven to be a very useful hypothesis.

The data plotted in Fig. 5 may be Abel inverted to provide the free electron density n_e of the FRC versus radius r, assuming an azimuthal symmetry. To preview further analysis, Fig. 6 plots the results for the subject shot for a range of times between 26 and 32 μs. The algorithm assumes a solution consisting of a continuous piecewise linear function for n_e when plotted against variable $u = r^2$ (hence the curvature when plotted against r), with vertices at radii equal to the probe impact parameters. It has been observed by diameter probing interferometry elsewhere[9] that the interferometric signal oscillations after 32 μs in Fig. 5 are the characteristic signature of an $n=2$ rotational instability that ends the azi-
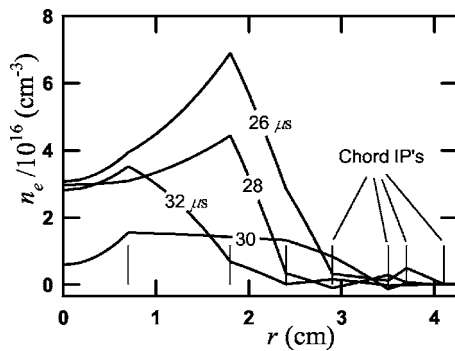
FIG. 6. Density n_e vs radius r at different (labeled) times of the representative shot via the Abel inversion. The vertical lines identify the chordal impact parameter values.

muthally symmetric interval. This interpretation is corroborated by previous researches which show that $n=2$ is dominant based on end-on imaging[10–12] and on theoretical analyses.[13–15] Details of the above Abel inversion algorithm, in addition to an alternate one that produces smooth curves for calculating gradients more accurately, tomographic inversions of the presented data set after the $n=2$ mode saturates, and basic FRC properties that may be inferred therefrom, are the subjects of the complementary paper mentioned in Sec. I.

In sum, design and data analysis issues for a multichord laser interferometer used to perform Abel and tomographic inversions of a rotating plasma are presented in sufficient detail to provide a valuable guide for others planning to build and field a similar instrument. Issues resolved during the instrument's development and data analysis such as protec-

tion of the electronic optical detection/demodulation circuit from rf noise and compensation for the cylindrical lensing of the probe beams due to the fused quartz tube comprising the FRC chamber, and their solutions are presented. Of particular note, a significant source of signal, apparently due to the interaction of plasma radiation with the tube wall, is described and accounted for by the hypothesis that it is primarily due to heating of the fused quartz bulk.

[1] T. Intrator *et al.*, Phys. Plasmas **11**, 2580 (2004).
[2] S. Zhang, T. P. Intrator, G. A. Wurden, W. J. Waganaar, J. M. Taccetti, R. Renneke, C. Grabowski, and E. L. Ruden, Phys. Plasmas **12**, 052513 (2005).
[3] M. Tuszewski, G. A. Barnes, R. E. Chrien, W. N. Hugrass, D. J. Rej, R. E. Siemon, and B. Wright, Phys. Fluids **31**, 946 (1988).
[4] J. M. Taccetti *et al.*, Rev. Sci. Instrum. **74**, 4314 (2003).
[5] W. S. Rodney and R. J. Spindler, J. Res. Natl. Bur. Stand. **53**, 185 (1954).
[6] R. H. Huddleston and S. L. Leonard, *Plasma Diagnostic Techniques* (Academic, New York, 1965), p. 479.
[7] W. Lochte-Holtgreven, *Plasma Diagnostics* (AIP, New York, 1995), p. 607.
[8] T. P. Intrator *et al.*, IEEE Trans. Plasma Sci. **32**, 152 (2004).
[9] T. Minato *et al.*, Plasma Phys. Controlled Nucl. Fusion Res. **2**, 303 (1983).
[10] W. T. Armstrong, R. K. Linford, D. A. Platts, and E. G. Sherwood, Phys. Fluids **24**, 2068 (1981).
[11] M. Tuszewski, Nucl. Fusion **28**, 2033 (1988).
[12] D. P. Taggart, R. J. Gribble, A. D. Bailey III, and S. Sugimoto, in *US-Japan Workshop on Field-Reversed Configurations with Steady-State High-Temperature Fusion Plasmas and the 11th US-Japan Workshop on Compact Toroids*, edited by D. C. Barnes, J. C. Fernández, and D. J. Rej (LANL, Los Alamos, NM, 1994), Report No. LA-11808-C, pp. 87–92.
[13] J. P. Freidberg and L. D. Pearlstein, Phys. Fluids **21**, 1207 (1978).
[14] C. E. Seyler, Phys. Fluids **22**, 2324 (1978).
[15] D. S. Harned, Phys. Fluids **26**, 1320 (1983).